Cell Surface Self-Assembly of Hybrid Nanoconjugates *via* Oligonucleotide Hybridization Induces Apoptosis

Te-Wei Chu[1], **Jiyuan Yang**[1], **Rui Zhang**[1], **Monika Sima**[1], and **Jindřich Kopeček**[1,2,*]

[1]Department of Pharmaceutics and Pharmaceutical Chemistry/Center for Controlled Chemical Delivery, University of Utah, Salt Lake City, Utah 84112, USA

[2]Department of Bioengineering, University of Utah, Salt Lake City, Utah 84112, USA

Abstract

Hybrid nanomaterials composed of synthetic and biological building blocks possess high potential for the design of nanomedicines. The use of self-assembling nanomaterials as "bio-mimics" may trigger cellular events and result in new therapeutic effects. Motivated by this rationale, we designed a therapeutic platform that mimics the mechanism of immune effector cells to crosslink surface receptors of target cells and induce apoptosis. This platform was tested against B-cell lymphomas that highly express the surface antigen CD20. Here, two nanoconjugates were synthesized: (1) an anti-CD20 Fab' fragment covalently linked to a single-stranded morpholino oligonucleotide (MORF1), and (2) a linear polymer of *N*-(2-hydroxypropyl)methacrylamide (HPMA) grafted with multiple copies of the complementary oligonucleotide MORF2. We show that the two conjugates self-assemble *via* MORF1-MORF2 hybridization at the surface of CD20$^+$ malignant B-cells, which crosslinks CD20 antigens and initiates apoptosis. When tested in a murine model of human non-Hodgkin's lymphoma, the two conjugates, either administered consecutively or as a premixture, eradicated cancer cells and produced long-term survivors. The designed therapeutics contains no small-molecule cytotoxic compounds and is immune-independent, aiming to improve over chemotherapy, radiotherapy and immunotherapy. This therapeutic platform can be applied to crosslink any non-internalizing receptor and potentially treat other diseases.

Keywords

biorecognition; receptor crosslinking; apoptosis; morpholino oligonucleotide; *N*-(2-hydroxypropyl)methacrylamide (HPMA); CD20; B-cell lymphoma

---

Molecular biorecognition is a fundamental feature of life – many biological processes are governed by the complex yet specific interactions between macromolecules, *e.g.*, antibody-antigen binding and DNA base pairing. These high-fidelity recognition motifs from nature can be employed to design self-assembling nanobiomaterials for applications in drug delivery,[1–3] tissue engineering,[4,5] bio-detection,[6–8] *etc*. A new direction of research is to use

such precisely defined "smart" materials to incite or control cellular activities;[9–11] in this case the materials alone, without any conventional drug, can provide therapeutic effects. Such biomimetic strategy translates molecular biorecognition into cellular responses to define new therapeutic entities with high functional specificity.

Non-Hodgkin's lymphoma (NHL) is a prevalent cancer worldwide with a high mortality rate.[12] Conventional chemotherapy and radiotherapy are accompanied by significant adverse reactions, particularly cytopenias leading to increased risk of infection and need for transfusions. Because most NHLs are of B-cell origin, immunotherapies using monoclonal antibodies (mAbs) targeted to the B-cell surface antigen CD20 have become common treatments.[13] However, large populations of patients exist who are not responsive to immunotherapies, especially in the relapse setting. For example, rituximab, the most commonly used anti-CD20 mAb, has a less than 50% overall response rate for relapsed/ refractory NHL.[14] This is largely attributed to the inactivity of immune effector cells to hyper-crosslink ligated mAbs.[15,16] Moreover, mAb treatments cause rare but lethal side effects such as progressive multifocal leukoencephalopathy[17] and lung injuries,[18,19] which are due to Fc-mediated effector cellular events (*e.g.* complement activation).[20] These clinical obstacles are calling for new, improved therapeutic strategies.

We designed a biomimetic material platform composed of self-assembling hybrid nanoconjugates (Figure 1A) as a therapeutic system against B-cell lymphomas (Figure 1B). It comprises an anti-CD20 Fab' antibody fragment, a pair of complementary phosphorodiamidate morpholino oligomers (MORF1 and MORF2), and a linear polymer (P) of *N*-(2-hydroxypropyl)methacrylamide (HPMA). We hypothesized that: (1) the exposure of malignant CD20$^+$ B-cells to the conjugate of anti-CD20 Fab' and MORF1 (Fab'-MORF1) decorates the cell surfaces with MORF1; and (2) further treatment of decorated B-cells with HPMA copolymer grafted with multiple copies of MORF2 (P-MORF2) results in MORF1-MORF2 hybridization at the cell surface with concomitant CD20 crosslinking, which triggers apoptosis. The proposed mechanism of apoptosis induction is shown in Figure 1B.

This design is inspired by the fact that cell surface receptor clustering is a driving force for numerous cellular events, *e.g.*, cell adhesion,[21] cell proliferation,[22] and hormone uptake.[23] In particular, when CD20-bound antibodies are hyper-crosslinked by Fc receptor (FcR)-expressing immune effector cells (*e.g.* macrophages, natural killer cells), CD20 clustering occurs within lipid rafts and induces apoptosis.[24] We named the designed platform "drug-free macromolecular therapeutics" due to the absence of low-molecular-weight drugs that are often toxic (*e.g.* chemotherapeutic agents).[9] Furthermore, each component (Fab', morpholino oligo, HPMA polymer) of this system, when used individually, does not have any pharmacological effect. The apoptosis induction is direct (*i.e.* independent of immune function) and specific (*i.e.* targeted to CD20); thus, it has the potential to address the side effect problems of currently used immunotherapy, chemo- and radiotherapy.

The design is based on a pair of morpholino (MORF) oligonucleotides with complementary sequences. They form double helixes by Watson-Crick base pairing (hybridization) and serve as physical crosslinkers. MORF oligos have a charge-neutral phosphorodiamidate backbone resulting in much stronger binding affinity than DNA or RNA.[25] More importantly, they are biocompatible and nuclease resistant; this ensures *in vivo* stability and safety.[26] Due to these advantages, MORF oligos have been successfully used as macromolecular binders to enhance therapeutic delivery.[2,27,28] The HPMA copolymers are water-soluble and long circulating in the bloodstream; they have well-established safety profiles and are used extensively as therapeutic carriers.[29] In aqueous solutions, linear HPMA copolymers have a random coil conformation and are able to effectively present targeting moieties that are grafted to the side chains.[30]

In this study, we show the development and preclinical evaluation of the proposed anti-lymphoma nanomedicine. Biorecognition of the two nanoconjugates (Fab'-MORF1 and P-MORF2) was characterized. The therapeutic system was optimized to achieve efficient apoptosis induction of malignant B-cell lines. Excellent anticancer efficacy (100% survival without residual tumors) was demonstrated in a mouse model of human NHL. These findings validate the concept of the designed therapeutic platform.

RESULTS AND DISCUSSION

To verify the concept of hybridization-mediated drug-free macromolecular therapeutics, we selected CD20 as a pharmacological target. CD20 is a non-internalizing receptor expressed on most NHL malignant B-cells as well as on normal B-cells.[31] However, it is not expressed on plasma cells (effector B-cells) and stem cells. Consequently, humoral immunity of patients is not severely affected, and normal numbers of B-cells can be restored after treatment.[32,33] Here, we employed an anti-CD20 Fab' fragment in the therapeutic system and used NHL as a disease model to demonstrate the first example of the designed platform.

Design of MORF1 and MORF2

The MORF oligos used in this study were 25 bp and about 8.5 kDa (see structure in Figure 2 and Supplementary Figure S1). Their 3' termini were modified with a primary amine used for conjugation. The A/T/C/G content was selected to achieve optimal binding efficacy and specificity (GC = 35–65%[26]), maintain aqueous solubility (G < 36%[26]), and potentially provide favorable pharmacokinetics (number of C < 7 to avoid rapid kidney uptake[27]). After the base composition was determined, the sequences were generated by a scrambling software to minimize off-target binding with human and murine mRNA and further optimized to prevent self-complementarity.

Synthesis and characterization of Fab'-MORF1 and P-MORF2

To prepare the Fab'-MORF1 conjugate (Figure 2A), the Fab' fragment from a mouse anti-human CD20 IgG2a mAb (1F5)[34] was tethered to the 3' end of MORF1 *via* a thioether bond. Optionally, the conjugates were labeled with rhodamine (RHO) for imaging studies. Fab'-MORF1 was successfully synthesized as confirmed by HPLC (Figure 2B) and size exclusion chromatography (SEC) (Supplementary Figure S2A); the coupling reaction followed a 1:1 stoichiometry as characterized by MALDI-ToF mass spectrometry (Supplementary Figure S2B) and UV-visible spectroscopy (Supplementary Figure S2C). The molecular weight (MW) of Fab'-MORF1 was about 57.5 kDa.

To prepare the multivalent P-MORF2 conjugates (Figure 2C), we first synthesized HPMA copolymers containing glycyl-glycine (GG; spacer) side-chains terminated in (amine-reactive) thiazolidine-2-thione (TT) groups. These polymer precursors (P-TT) were synthesized by reversible addition-fragmentation chain transfer (RAFT) polymerization. A polymerizable fluorescein isothiocyanate (FITC) derivative was optionally added for imaging studies. Using RAFT polymerization, polymer backbones with narrow MW distribution (polydispersity index   1.15, as determined by SEC) were reproducibly synthesized. Furthermore, the amine-derivatized MORF2 oligos (MORF2-NH$_2$) were grafted *via* stable amide linkage to the side chains of the HPMA copolymers to produce multivalent P-MORF2. The conjugates were purified and characterized by SEC (Figure 2D). Three different P-MORF2's with varying backbone MW and valences (number of MORF2 per polymer chain) were synthesized; see Supplementary Figure S3 for details. The backbone number average molecular weights (Mn) of these conjugates ranged from 70 to 136 kDa. Valences of the three P-MORF2 conjugates were 2, 3 and 10, respectively.

In vitro hybridization of Fab'-MORF1 and P-MORF2

Hybridization of the two conjugates *via* MORF1-MORF2 biorecognition was first evaluated by UV-visible spectroscopy. The two conjugates were mixed in different ratios, and the optical density at 260 nm (contributed by bases) was measured. Upon mixing Fab'-MORF1 and P-MORF2, a "hypochromic effect" was observed (Figure 3A); the OD_{260nm} reached a minimum when a molar ratio of 1:1 (MORF1:MORF2) was used. Such decrease was due to hydrogen bonding between complementary bases that limited the resonance of the aromatic rings. This method was also used to determine hybridization of the free, unconjugated MORF1 and MORF2, and the same hypochromicity was observed (Supplementary Figure S4). These results indicated that the function of MORF1-MORF2 hybridization was preserved after conjugation to Fab' or polymers.

Furthermore, the binding of Fab'-MORF1 and P-MORF2 was characterized by dynamic light scattering (DLS) (Figure 3B and Supplementary Figure S5). As shown in Figure 3B, a significant and rapid increase of hydrodynamic size upon mixing the two conjugates (at equimolar MORF1/MORF2) was revealed. The fast attainment of stable diameter (~40 nm) reflected a fast binding kinetics (< 10 min) of MORF1-MORF2 hybridization of the conjugates. Such rapid binding is in agreement with the literature; for example, Mang'era *et al.* reported that a pair of 15-mer complementary MORF oligomers reached near-maximal binding within 2–5 min.[28] This characteristic is favorable for the design of drug-free macromolecular therapeutics.

Circular dichroism (CD) spectroscopy was used to determine the melting temperature (Tm) of the Fab'-MORF1/P-MORF2 complex in physiological conditions (PBS pH=7.4) (Figure 3C). First, a pronounced optical signature (maximum at 260 nm, minimum at 210 nm) indicating A-form double helixes[35] was obtained upon mixing the two conjugates; a similar CD profile was observed when unconjugated MORF1 and MORF2 were mixed (Supplementary Figure S6). Second, a thermal melting study was performed to analyze the mixture of Fab'-MORF1 and P-MORF2. Data showed that the aforementioned CD signature no longer existed at 95 °C; the positive band at 260 nm underwent a significant bathochromic shift that produced a peak centered around 275 nm (Supplementary Figures S7 and S8). The thermo-melting curve shown in Figure 3C demonstrates that the signal at 260 nm decreased in a sigmoidal pattern as temperature increased. Results of nonlinear regression indicated a Tm value of about 57 to 62 °C. The Tm is well above body temperature, suggesting *in vivo* stability of the binding.

Biorecognition of Fab'-MORF1 and P-MORF2 at B-cell surface

Human B-cell lymphoma Raji cell line (CD20+)[31,36] was used to study the biorecognition of Fab'-MORF1 and P-MORF2 at the cell surface. This study was performed by confocal fluorescence microscopy. First, exposure of Raji cells to rhodamine-labeled Fab'-MORF1 resulted in cell surface red signal (RHO) decoration due to Fab'-MORF1 binding to CD20; cells exposed to only FITC-labeled P-MORF2 did not show any fluorescent signal (Figure 4A). Second, when Raji cells were exposed to both fluorescently labeled conjugates (Fab'-MORF1 + P-MORF2), either consecutively or as a premixture, the red and the green (FITC) signals were well co-localized at the surfaces of B-cells (Figure 4B). This observation indicated successful MORF1-MORF2 hybridization at cell surface. Figure 4C shows the microscopic images obtained from two control groups: (1) cells exposed to the premixture of Fab'-MORF1(-RHO) and an HPMA copolymer carrying FITC dye but without MORF2 (P-FITC); (2) a "pre-blocking" control achieved by exposing cells consecutively to Fab'-MORF1(-RHO) followed by a mixture of P-MORF2(-FITC) with an excess of unconjugated MORF1 (this produced HPMA copolymers grafted with double-stranded MORF; P-dsMORF). As expected, both control treatments resulted in only the red signal at cell

surfaces (Figure 4C) due to absence of a biorecognition pair. Results of these controls confirmed that the cell surface biorecognition of Fab'-MORF1 and P-MORF2 was indeed mediated by MORF1-MORF2 hybridization.

Apoptosis induction of human NHL B-cells

Apoptosis induction of human B-cell lines (Raji and DG75) was evaluated by three methods: caspase-3 activation assay, annexin V/propidium iodide (PI) binding assay, and terminal deoxynucleotidyl transferase dUTP nick end-labeling (TUNEL) assay. Throughout these studies, anti-CD20 1F5 mAb hyper-crosslinked with a goat anti-mouse secondary Ab (2° Ab) was used as a positive control to imitate the function of FcR[+] immune effector cells.[36] This control partly reflects the therapeutic efficacy of anti-CD20 mAbs. Results showed that co-treatment with Fab'-MORF1 and P-MORF2, either consecutively or as a premixture, effectively induced apoptosis of Raji B-cells (Figure 5). In contrast, single-component treatments with either Fab'-MORF1 or P-MORF2 failed to initiate apoptosis. A series of control experiments validated the hypothesis that MORF1-MORF2 hybridization with concomitant crosslinking of CD20 antigens is responsible for the apoptosis induction. Raji cells were exposed to: (1) a mixture of Fab'-MORF1 and the polymer precursor P-TT; (2) a mixture of Fab' and P-MORF2; (3) "pre-blocked" conjugates whose MORF1 or MORF2 binding sites were blocked by excess unconjugated complementary MORFs prior to treatment. None of these treatments induced apoptosis, due to absence of MORF1-MORF2 hybridization (Supplementary Figure S9A). Furthermore, the apoptosis of a negative control B-cell line (DG75) that does not (or minimally) express CD20 was evaluated.[37] The levels of apoptosis after co-treatment with two nanoconjugates were very low, and similar to that of the untreated cells (Supplementary Figure S9B). This result indicated that CD20 binding is a necessary event for apoptosis induction.

Optimization of apoptosis induction

To optimize the therapeutic system, several factors and their impact on apoptosis of Raji B-cells were examined, including concentration of conjugates, ratio between two conjugates, valence of P-MORF2, and exposure time. We started with a P-MORF2 containing about 3 oligos per polymer chain (P-MORF2/v3). Results of annexin V/PI staining assay indicated that 1 μM Fab'-MORF1 and equimolar P-MORF2/v3 (MORF1:MORF2=1:1) induced about 40% apoptotic cells (more than 4 fold compared to untreated) (Figure 5A). When all conditions were kept identical except different concentrations of Fab'-MORF1 (and corresponding P-MORF2/v3), a concentration-dependent apoptosis induction was observed (Figure 5B). Data suggested that increasing concentrations of the conjugates from 0.5 μM to 2 and 5 μM (Fab' equivalent) resulted in higher levels of apoptosis. The dose-dependent trends were observed in both consecutive and premixed treatment regimens as well as in the positive control (mAb + 2° Ab). At the highest concentration tested (5 μM), apoptosis induction by drug-free macromolecular therapeutics (Fab'-MORF1 + P-MORF2/v3) reached about 7 fold compared to untreated controls. In addition, the percentage of the apoptotic cells induced by mAb + 2° Ab seemed to saturate when the concentration of 1F5 mAb was increased from 2 to 5 μM; however, such saturation was not observed in the nanomedicine groups. This difference was likely due to P-MORF2 having multimeric interactions with targets, in contrast to mAbs with only two binding sites.

Furthermore, we examined the influence of the valence of P-MORF2 and the ratio between Fab'-MORF1 and P-MORF2 on apoptosis induction of Raji B-cells. A "high-valence" P-MORF2 containing 10 oligos per chain (P-MORF2/v10) was compared with P-MORF2/v3 (3 oligos per chain). Results showed that when all treatment conditions were identical (0.5 μM Fab', MORF1:MORF2=1:1 or 1:10), the P-MORF2/v10 conjugate induced about 2-fold higher levels of apoptosis comparing to P-MORF2/v3 (Figure 5C). It is noteworthy that the

consecutive treatment of Fab'-MORF1 and P-MORF2/v10 induced apoptosis more effectively than the positive control (consecutive treatment of mAb and 2° Ab). The superior apoptosis induction observed here was likely due to multivalency of P-MORF2/v10 resulting in higher avidity to B-cells as well as more effective CD20 clustering.[38–40] Interestingly, when Raji cells were exposed to the same concentration of Fab'-MORF1 (0.5 μM), whereas a 10-time excess P-MORF2 was used (MORF1:MORF2=1:10), we did not observe significantly enhanced apoptotic levels compared to the treatment with equimolar MORF1/MORF2 (Figure 5C). Apparently, the MORF1 binding sites on the surfaces of the Fab'-MORF1-decorated cells were saturated, which suggests good accessibility of MORFs on the polymer chain for hybridization (minimal steric hindrance effect by the polymer chain). The same trends of apoptosis induction were observed at different exposure times and from different apoptosis assays (Supplementary Figure S10).

Preclinical evaluation in a murine model of human NHL

In vivo therapeutic efficacy of the hybridization-mediated drug-free macromolecular therapeutics was evaluated in SCID (C.B-17) mice bearing systemically disseminated Raji B-cells. This animal model has a near 100% tumor engraftment rate,[41] and the hind-limb paralysis-free survival time after treatment accurately reflects anticancer efficacy.[42,43] The conjugates, Fab'-MORF1 and P-MORF2/v10, were injected *via* the tail vein of mice either consecutively or as a premixture. Mice divided into different groups (n=6–7) received either one or three doses of the nanomedicine, starting at 24 h after tumor injection. Doses and treatment regimens were based on literature[42,43] and our previous study with peptide conjugates.[44] The animal survival curve is shown in Figure 6. The negative control mice treated with PBS (n=8) developed hind-limb paralysis in 17–35 days after injection of cancer cells; the median survival time was 24 days. This observation was in agreement with the literature.[43,44] A single administration of the consecutive treatment (Cons ×1; MORF1:MORF2=1:1) substantially extended the animal survival (median survival time: 81 days). A single premixed dose (Prem ×1; MORF1:MORF2=1:1) had similar efficacy as the consecutive treatment, resulting in a median survival of 78 days. When the same dose of Fab'-MORF1 (57.5 μg/20 g) was given but followed by a 5-time excess P-MORF2/v10 (MORF1:MORF2=1:5), the efficacy significantly improved over the treatment with equimolar MORF1/MORF2. A single administration of such treatment (Cons (1:5) ×1) produced a 67% survival rate (4/6 long-term survivors; 125 days). The discrepancy between *in vivo* and *in vitro* data (Figure 5C), when excess P-MORF2 was used, can be explained by blood dilution of the conjugates, which interferes with binding saturation.

Excellent therapeutic efficacy was observed with the groups of mice that received 3 consecutive administration doses (Cons ×3; n=7) or 3 premixed administration doses (Prem ×3; n=7). All mice survived until the experimental endpoint (day 125). The positive control group (n=7) that received 3 equivalent doses of 1F5 mAb (*i.v.*) had an 86% survival rate. Although the difference to the 3-dose nanomedicine groups is not statistically significant, the anticancer activity of the nanomedicine, unlike mAbs, is independent of immune effector mechanisms such as antibody-dependent cellular cytotoxicity (ADCC) and complement-dependent cytotoxicity (CDC).[45] These data indicated that the direct apoptosis induction strategy can be as effective as the immunotherapy while simultaneously reducing the concerns of side effects that are mostly associated with ADCC and CDC.[20,45] The preclinical evaluation here demonstrated the *in vivo* anticancer efficacy of the hybridization-mediated drug-free macromolecular therapeutics and suggested that the therapeutic efficacy can be further improved by increasing the number of treatments and/or the dose of the second, therapeutically active conjugate (P-MORF2).

Analysis of *in vivo* anti-lymphoma efficacy

Using the above-mentioned animal model, eradication of Raji cells in SCID mice after treatment with Fab'-MORF1 and P-MORF2 was confirmed by MRI, flow cytometry and histology. MRI with gadolinium-based contrast at 4–5 weeks after injection of cancer cells showed that the control mice treated with PBS developed tumors in the lumbar spinal cord, whereas three doses of the nanomedicine prevented tumor development (Figure 7A). The surviving mice treated with Cons ×3 or Prem ×3 were imaged again on week-16; no relapse of the disease was observed (Supplementary Figure S11). After the mice were sacrificed, flow cytometry was performed to analyze residual Raji cells (human CD10$^+$ CD19$^+$) in the femoral bone marrow (Figure 7B). Two fluorescently labeled antibodies, PE-labeled mouse anti-human CD10 and APC-labeled mouse anti-human CD19, were used for flow cytometry analysis.[46] Results indicated that the paralyzed animals (PBS-treated) bore significant amounts of Raji cells in the bone marrow, while all long-term survivors in the therapy groups (Cons ×3 and Prem ×3) were tumor free (Figure 7C). Flow cytometry also confirmed Raji cells in the spinal cord of paralyzed mice (PBS-treated), but not in the long-term survivors (Supplementary Figure S12), which was in agreement with MRI data. Furthermore, histological examination disclosed lymphoma dissemination in the liver, lung and brain of PBS-treated mice (Figure 8). In contrast, no tumors were found in the long-term survivors. Importantly, histology suggested no toxicity caused by the treatments in any of the tissues evaluated; this corresponded to a stable body weight growth of the treated animals (Supplementary Figure S13). These results in conjunction indicated that the nanomedicine successfully inhibited lymphoma cell growth/dissemination *in vivo* without acute toxicity.

CONCLUSIONS

Data presented here validate the proposed concept of hybridization-mediated cell surface antigen crosslinking and apoptosis induction. A unique bio-inspired nanomaterial system has been demonstrated where extracellular hybridization of oligonucleotide analogues translates into innate biological responses. The cellular event (apoptosis) is triggered by specific biorecognition defined from the molecular level (*i.e.* base pairing), suitable for the design of precisely targeted therapeutics. The proposed two-step (consecutive) treatment offers the opportunity of pretargeting.[47–49] This is an advantage over the premixed treatment and other single-component anti-CD20 constructs, such as rituximab polymers[50] and multivalent anti-CD20 Fab'-functionalized polymers.[38–40] For example, the timing of administration of the crosslinking dose (P-MORF2) can be optimized based on biodistribution of the pretargeting dose (Fab'-MORF1), in order to achieve maximal tumor-to-tissue accumulation in individual patients and enable more efficient treatment. This approach would also limit potential adverse reactions associated with off-target binding, thus being beneficial for the treatment of solid tumors as well as disseminated diseases. For blood-based cancers, the pharmacokinetics of Fab'-MORF1 and the binding kinetics of Fab'-MORF1 to diseased cells can be further studied to determine the best timing for P-MORF2 administration.

The presented work offers a new strategy in lymphoma treatment by immune-independent apoptosis induction. This is a potential improvement over currently used immunotherapies with type I anti-CD20 mAbs (*e.g.* rituximab).[14,16] Comparing to type II anti-CD20 mAbs (*e.g.* obinutuzumab) that may also induce direct apoptosis,[51] our nanomedicine approach still possesses two advantages: (1) superior targeting of B-cells due to multivalency, and (2) potential for decreased side effects that are associated with immune functions. Previously our lab has designed and developed a pilot anti-CD20 drug-free macromolecular therapeutic system using a pair of pentaheptad peptides that formed antiparallel coiled-coil heterodimers as the biorecognition moieties.[9,44] When compared to this previous design using peptides,

the MORF oligos clearly demonstrated faster binding kinetics as well as more efficient binding (equimolar MORF1/MORF2 reached binding saturation *in vitro*), therefore resulting in superior apoptosis induction and *in vivo* anti-lymphoma efficacy (see Supplementary Discussion in SI for details).

Besides lymphomas, the therapeutic conjugates developed here can be used for other B-cell-associated diseases such as rheumatoid arthritis, multiple sclerosis, and chronic lymphocytic leukemia. The designed platform can be applied to crosslink any non- or slowly internalizing receptor (*e.g.* CD45,[52] prostate stem cell antigen[53]) and control different cellular activities.[21–23] In addition, other targeting moieties (*e.g.* aptamer instead of Fab')[49] can be used to construct various self-assembling antigen crosslinkers. Therefore, this work constitutes a new paradigm of nanomaterial-based therapeutics with significant potential for the treatment of multiple different diseases.

MATERIALS AND METHODS

MORF1 and MORF2

The two complementary 3'-amine-derivatized 25-mer phosphorodiamidate morpholino oligomers were from Gene Tools, LLC (Philomath, OR). MORF1: 5'-GAGTAAGCCAAGGAGAATCAATATA-linker-amine-3' (MW=8630.5 Da); MORF2: 5'-TATATTGATTCTCCTTGGCTTACTC-linker-amine-3' (MW=8438.5 Da). Structure of the linker is shown in Supplementary Figure S1. For the design of base sequences, a sequence scrambling software (http://www.sirnawizard.com/scrambled.php) and a sequence analysis software (http://www.basic.northwestern.edu/biotools/oligocalc.html) were used.

Preparation of Fab'-MORF1

The 1F5 mAb was prepared from a murine hybridoma cell sub-clone 1F5 (ATCC, Bethesda, MD) in a CellMax® bioreactor (Spectrum Laboratories, Rancho Dominguez, CA). Antibodies were harvested from the culture media, and purified on a Protein G Sepharose 4 Fast Flow column (GE Healthcare, Piscataway, NJ). Preparation of Fab' from mAb followed a previously reported procedure.[54] Briefly, mAb was digested into $F(ab')_2$ with 10% (w/w) pepsin (Sigma, St. Louis, MO) in citric buffer (pH 4.0). Immediately before conjugation, $F(ab')_2$ was reduced to Fab' by 10 mM tris(2-carboxyethyl)phosphine (Thermo Scientific, Waltham, MA). To prepare the Fab'-MORF1 conjugate, the MORF1 oligo containing a 3'-primary amine was reacted with succinimidyl-4-(*N*-maleimidomethyl)cyclohexane-1-carboxylate (SMCC) to introduce a terminal (thiol-reactive) maleimide group. This produced MORF1 with 3'-maleimide (MORF1-mal). MORF1-mal was then conjugated to Fab' (containing a terminal thiol group) *via* a thioether bond to obtain Fab'-MORF1. The conjugates were purified using SEC to remove free, unconjugated Fab' and MORF1. For detailed procedures regarding the synthesis and characterization of Fab'-MORF1, see Supporting Information.

Preparation of P-MORF2

The polymer precursors (P-TT and P-TT-FITC), namely, copolymers of *N*-(2-hydroxypropyl)methacrylamide (HPMA), *N*-methacryloylglycylglycine thiazolidine-2-thione (MA-GG-TT), and optionally *N*-methacryloylaminopropyl fluorescein thiourea (MA-FITC), were synthesized by RAFT copolymerization. 2,2'-Azobis[2-(2-imidazolin-2-yl)propane]dihydrochloride (VA-044; Wako Chemicals, Richmond, VA) was used as the initiator, and 4-cyanopentanoic acid dithiobenzoate (CPDB) as the chain transfer agent. CPDB[55] and monomers HPMA,[56] MA-GG-TT,[57] and MA-FITC[58] were synthesized as previously described. For detailed procedures regarding the RAFT copolymerization and the synthesis and characterization of P-MORF2, see Supporting Information.

Quantification of Fab'-MORF1 and P-MORF2

UV-visible spectroscopy was used for quantification of MORF1 and MORF2 oligos, as well as determination of the content of MORFs in the conjugates. The molar absorptivities of MORF1 and MORF2 (at 265 nm, in 0.1 N HCl) were 278,000 and 252,000 (M^{-1} cm^{-1}), respectively. The valence of the P-MORF2 conjugates was determined using the extinction coefficient of MORF2 and the Mn's of the polymer backbones; see Supporting Information for details. The MORF2 equivalent concentration of P-MORF2 conjugates was quantified using UV-visible spectroscopy. The Fab' equivalent concentration of the Fab'-MORF1 conjugate was quantified by the bicinchoninic acid (BCA) protein assay (Thermo Scientific Pierce, Rockford, IL).

Confocal fluorescence microscopy

Human Burkitt's B-cell non-Hodgkin's lymphoma Raji cell line (ATCC, Bethesda, MD) was cultured in RPMI-1640 medium (Sigma, St. Louis, MO) supplemented with 10% fetal bovine serum (Hyclone, Logan, UT) at 37 °C in a humidified atmosphere with 5% CO_2 (v/v). All experiments were performed using cells in exponential growth phase. For the consecutive treatment, cells at a density of 10^6 per well were incubated with 0.4 mL Fab'-MORF1-RHO (0.4 μM Fab' equivalent) in culture medium at 37 °C for 1 h; then the cells were washed twice with PBS prior to incubation with 0.4 mL of P-MORF2-FITC (0.4 μM MORF2 equivalent) for another 1 h. For the premixed treatment, Fab'-MORF1-RHO and P-MORF2-FITC were firstly mixed in culture medium in equimolar concentrations (0.4 μM) for 1 h; then cells at the same density were incubated with 0.4 mL of the premixture solution for 1 h. After incubation, the cells were washed twice with PBS (to discard the media that contained the conjugates), and then plated onto sterile 35-mm glass bottom dishes with 14-mm microwells (MatTek Corporation, Ashland, MA) for imaging, using Olympus laser scanning confocal microscope (FV 1000). For control studies, concentrations of all corresponding components were kept consistent; excess amounts of P-FITC and P-dsMORF were used. Prior to analysis, cells incubated with FITC-labeled 1F5 mAb, rhodamine-labeled F(ab')$_2$, and PBS were used to adjust channel setting and confirm CD20 binding.

In vitro apoptosis evaluation

Apoptosis of human NHL B-cells was evaluated by three methods: caspase-3 assay, annexin V/PI assay, and TUNEL assay. These assays evaluated apoptosis from different aspects – levels of caspase-3 activation represented apoptotic protein expression; annexin V/PI binding characterized cell membrane flipping as an early apoptotic event; TUNEL assay analyzed genomic DNA fragmentation as a late apoptotic event. Quantification of apoptotic activity (% apoptotic cells) was performed by flow cytometry. For detailed procedures of each assay, see Supporting Information.

In vivo anticancer efficacy

Female C.B-17 SCID mice (Charles River Laboratories, Wilmington, MA) at about 7 weeks of age were intravenously injected with 4×10^6 Raji cells in 200 μL saline *via* the tail vein (day 0). This animal model represents dissemination, infiltration and growth of lymphoma cells in various organs, including spinal cord that leads to hind-limb paralysis and subsequent animal death.[41–43] The onset of hind-limb paralysis was the experimental end point; in addition, mice were sacrificed when body weight loss was > 20%. Animals without signs of paralysis/sickness were kept until 125 days and considered long-term survivors. The conjugates, Fab'-MORF1 (57.5 μg/20 g; 1 nmol MORF1) and P-MORF2/v10 (22 μg/20 g; 1 nmol MORF2), were dissolved in 100 μL PBS and injected *via* tail vein either consecutively (1-h interval) or as a premixture (mixed 1 h prior to treatment). The inoculated mice were divided into seven groups: (1) negative control (injected with 200 μL PBS), (2) single

administration of the consecutive treatment (Cons ×1), (3) single administration of the premixed treatment (Prem ×1), (4) consecutive treatment administered three times (Cons ×3), (5) premixed treatment administered three times (Prem ×3), (6) single administration of the consecutive treatment but with 5× excess P-MORF2/v10 (110 μg/20 g; 5 nmol MORF2) to Fab'-MORF1 (Cons (1:5) ×1), and (7) positive control injected with 3 doses (75 μg/20 g; 1 nmol Fab'-equivalent per dose) of 1F5 mAb *via* tail vein. For single-dose groups, conjugates were administered on day 1 (24 h after injection of cancer cells); for multiple-dose groups, conjugates (or mAb) were given on days 1, 3 and 5. To monitor disease progression, mice (2–4 per group) were scanned by T_1-weighted MRI on weeks 4, 5 and 16. Gadobenate dimeglumine (MultiHance®; Bracco SpA, Milan, Italy) was injected (*i.v.*) at 0.3 mmol/kg 20 min prior to imaging. Pre-contrast images were used for comparison. See Supporting Information for detailed MRI procedures. All animal experiments were performed according to the protocol approved by the Institutional Animal Care and Use Committee (IACUC) of the University of Utah.

Flow cytometry analysis of residual Raji cells

After mice were sacrificed, the following organs/tissues were analyzed by flow cytometry for residual Raji cells: bone marrow (femur), mesenteric and inguinal lymph nodes, spinal cord, and spleen. Two fluorescently labeled antibodies, R-phycoerythrin (PE)-labeled mouse anti-human CD10 (IgG1, κ isotype) and allophycocyanin (APC)-labeled mouse anti-human CD19 (IgG1, κ isotype) (BD Biosciences, San Jose, CA), were used to stain Raji B-cells.[46] Single-cell suspensions were prepared from the organs/tissues using the following procedures. For bone marrow, fresh femurs were purged with 1 mL PBS to obtain cell suspensions. Cells were resuspended in 5 mL red blood cell (RBC) lysis buffer and incubated at RT for 5 min. Cells were then washed with 5 mL PBS and centrifuged to remove debris, followed by resuspension in 400 μL cold washing buffer and equally divided into 4 tubes: (1) non-stained control, (2) CD10 singly-stained, (3) CD19 singly-stained, and (4) CD10/CD19 doubly-stained cells. For the staining, 20 μL of each antibody was added to 100 μL cell suspension containing about 10^6 cells. Cells were incubated for 30 min at 4 °C in the dark, and washed with 1.5 mL washing buffer prior to analysis. For lymph nodes, spinal cord and spleen, a mechanical method was used. Tissues were gently disaggregated with the help of tweezers in a Petri dish containing 1 mL PBS. The suspensions were passed through a 70-μm Falcon™ cell strainer (BD Biosciences) to remove large clumps and debris, and then cells were centrifuged and resuspended in 5 mL RBC lysis buffer. The rest of the procedures were the same as aforementioned. For flow cytometry analysis, data of $1–1.5 \times 10^5$ cells were recorded.

Pathological and histopathological examinations

Immediately after mice were sacrificed, the following organs/tissues were harvested for pathological evaluation: brain, heart, lung, liver, spleen, kidneys, spinal cord and lymph nodes. These organs/tissues were fixed in 10% formalin overnight at RT, and then transferred and preserved in 70% ethanol. Histopathological examination was performed by a blinded veterinary pathologist at ARUP Laboratories (Salt Lake City, UT). Sections were cut at 4-μm thickness, mounted on glass slides, and stained by hematoxylin and eosin (H&E).

Statistical analysis

All experiments in this study were at least triplicated. Quantified data were presented as mean ± standard deviation (SD). Statistical analyses were performed by Student's *t* test to compare between two groups, or one-way analysis of variance (ANOVA) to compare three

or more groups (with *p* value < 0.05 indicating statistically significant difference). Animal survival analysis was performed with the log-rank test using the GraphPad Prism 5 software.

Supplementary Material

Refer to Web version on PubMed Central for supplementary material.

Acknowledgments

REFERENCES AND NOTES

1. Douglas SM, Bachelet I, Church GM. A Logic-Gated Nanorobot for Targeted Transport of Molecular Payloads. Science. 2012; 335:831–834. [PubMed: 22344439]

2. Mulvey JJ, Villa CH, McDevitt MR, Escorcia FE, Casey E, Scheinberg DA. Self-Assembly of Carbon Nanotubes and Antibodies on Tumours for Targeted Amplified Delivery. Nat. Nanotechnol. 2013; 8:763–771. [PubMed: 24077028]

3. Lu ZR, Kope ková P, Kope ek J. Polymerizable Fab' Antibody Fragments for Targeting of Anticancer Drugs. Nat. Biotechnol. 1999; 17:1101–1104. [PubMed: 10545917]

4. Gungormus M, Branco M, Fong H, Schneider JP, Tamerler C, Sarikaya M. Self Assembled Bi-Functional Peptide Hydrogels with Biomineralization-Directing Peptides. Biomaterials. 2010; 31:7266–7274. [PubMed: 20591477]

5. Holmes TC, de Lacalle S, Su X, Liu G, Rich A, Zhang S. Extensive Neurite Outgrowth and Active Synapse Formation on Self-Assembling Peptide Scaffolds. Proc. Natl. Acad. Sci. U.S.A. 2000; 97:6728–6733. [PubMed: 10841570]

6. Yuan W, Yang J, Kope ková P, Kope ek J. Smart Hydrogels Containing Adenylate Kinase: Translating Substrate Recognition into Macroscopic Motion. J. Am. Chem. Soc. 2008; 130:15760–15761. [PubMed: 18980321]

7. Ehrick JD, Deo SK, Browning TW, Bachas LG, Madou MJ, Daunert S. Genetically Engineered Protein in Hydrogels Tailors Stimuli-Responsive Characteristics. Nat. Mater. 2005; 4:298–302. [PubMed: 15765106]

8. Liu J, Mazumdar D, Lu Y. A Simple and Sensitive "Dipstick" Test in Serum Based on Lateral Flow Separation of Aptamer-Linked Nanostructures. Angew. Chem. Int. Ed. 2006; 45:7955–7959.

9. Wu K, Liu J, Johnson RN, Yang J, Kope ek J. Drug-Free Macromolecular Therapeutics: Induction of Apoptosis by Coiled-Coil-Mediated Cross-Linking of Antigens on the Cell Surface. Angew. Chem. Int. Ed. 2010; 49:1451–1455.

10. Cho MH, Lee EJ, Son M, Lee JH, Yoo D, Kim JW, Park SW, Shin JS, Cheon J. A Magnetic Switch for the Control of Cell Death Signalling in *In Vitro* and *In Vivo* Systems. Nat. Mater. 2012; 11:1038–1043. [PubMed: 23042417]

11. Kope ek J, Yang J. Smart Self-Assembled Hybrid Hydrogel Biomaterials. Angew. Chem. Int. Ed. 2012; 51:7396–7417.

12. Siegel R, Naidsham D, Jemal A. Cancer Statistics 2013. CA Cancer. J. Clin. 2013; 63:11–30. [PubMed: 23335087]

13. Cheson BD, Leonard JP. Monoclonal Antibody Therapy for B-Cell Non-Hodgkin's Lymphoma. N. Engl. J. Med. 2008; 359:613–626. [PubMed: 18687642]

14. Molina A. A Decade of Rituximab: Improving Survival Outcomes in Non-Hodgkin's Lymphoma. Annu. Rev. Med. 2008; 59:237–250. [PubMed: 18186705]

15. Cartron G, Dacheux L, Salles G, Solala-Celigny P, Bardos P, Colombat P, Watier H. Therapeutic Activity of Humanized Anti-CD20 Monoclonal Antibody and Polymorphism in IgG Fc Receptor FcγRIIIa Gene. Blood. 2002; 99:754–758. [PubMed: 11806974]

16. Smith MR. Rituximab (Monoclonal Anti-CD20 Antibody): Mechanisms of Action and Resistance. Oncogene. 2003; 22:7359–7368. [PubMed: 14576843]

17. Allison M. PML Problems Loom for Rituxan. Nat. Biotechnol. 2010; 28:105–106. [PubMed: 20139927]

18. Lands LC. New Therapies, New Concerns: Rituximab-Associated Lung Injury. Pediatr. Nephrol. 2010; 25:1001–1003. [PubMed: 20195643]

19. Kamei K, Ito S, Iijima K. Severe Respiratory Adverse Events Associated with Rituximab Infusion. Pediatr. Nephrol. 2010; 25:1193. [PubMed: 20024586]

20. van der Kolk LE, Grillo-López AJ, Baars JW, Hack CE, van Oers MH. Complement Activation Plays a Key Role in the Side-Effects of Rituximab Treatment. Br. J. Haematol. 2001; 115:807–811. [PubMed: 11843813]

21. Shimizu Y, van Seventer GA, Ennis E, Newman W, Horgan KJ, Shaw S. Crosslinking of the T Cell-Specific Accessory Molecules CD7 and CD28 Modulates T Cell Adhesion. J. Exp. Med. 1992; 175:577–582. [PubMed: 1370688]

22. Vallat LD, Park Y, Li C, Gribben JG. Temporal Genetic Program Following B-Cell Receptor Cross-Linking: Altered Balance Between Proliferation and Death in Healthy and Malignant B Cells. Blood. 2007; 109:3989–3997. [PubMed: 17234734]

23. Kahn CR, Baird KL, Jarrett DB, Flier JS. Direct Demonstration That Receptor Crosslinking or Aggregation Is Important in Insulin Action. Proc. Natl. Acad. Sci. U.S.A. 1978; 75:4209–4213. [PubMed: 279910]

24. Deans JP, Li H, Polyak MJ. CD20-Mediated Apoptosis: Signalling through Lipid Rafts. Immunology. 2002; 107:176–182. [PubMed: 12383196]

25. Nielsen PE. DNA Analogues with Nonphosphodiester Backbones. Annu. Rev. Biophys. Biomol. Struct. 1995; 24:167–183. [PubMed: 7663113]

26. Summerton J, Weller D. Morpholino Antisense Oligomers: Design, Preparation, and Properties. Antisense Nucleic Acid Drug Dev. 1997; 7:187–195. [PubMed: 9212909]

27. Liu G, He J, Dou S, Gupta S, Vanderheyden JL, Rusckowski M, Hnatowich DJ. Pretargeting in Tumored Mice with Radiolabeled Morpholino Oligomer Showing Low Kidney Uptake. Eur. J. Nucl. Med. Mol. Imaging. 2004; 31:417–424. [PubMed: 14691611]

28. Mang'era KO, Liu G, Yi W, Zhang Y, Liu N, Gupta S, Rusckowski M, Hnatowich DJ. Initial Investigations of ^{99m}Tc-Labeled Morpholinos for Radiopharmaceutical Applications. Eur. J. Nucl. Med. 2001; 28:1682–1689. [PubMed: 11702111]

29. Kope ek J, Kope ková P. HPMA Copolymers: Origins, Early Developments, Present, and Future. Adv. Drug Deliv. Rev. 2010; 62:122–149. [PubMed: 19919846]

30. Ulbrich K, Šubr V. Structural and Chemical Aspects of HPMA Copolymers As Drug Carriers. Adv. Drug Deliv. Rev. 2010; 62:150–166. [PubMed: 19931329]

31. Stashenko P, Nadler LM, Hardy R, Schlossman SF. Characterization of a Human B Lymphocyte-Specific Antigen. J. Immunol. 1980; 125:1678–1685. [PubMed: 6157744]

32. Anderson KC, Bates MP, Slaughenhoupt BL, Pinkus GS, Schlossman SF, Nadler LM. Expression of Human B Cell-Associated Antigens on Leukemias and Lymphomas: A Model of Human B Cell Differentiation. Blood. 1984; 63:1424–1433. [PubMed: 6609729]

33. Kimby E. Tolerability and Safety of Rituximab (MabThera®). Cancer Treat. Rev. 2005; 31:456–473. [PubMed: 16054760]

34. Press OW, Appelbaum F, Ledbetter JA, Martin PJ, Zarling J, Kidd P, Thomas ED. Monoclonal Antibody 1F5 (Anti-CD20) Serotherapy of Human B Cell Lymphomas. Blood. 1987; 69:584–591. [PubMed: 3492224]

35. Johnson, WC. CD of Nucleic Acids. In: Berova, N.; Nakanishi, K.; Woody, RW., editors. Circular Dichroism: Principles and Applications. ed. 2. New York: Wiley-VCH; 2000. p. 703-718.

36. Shan D, Ledbetter JA, Press OW. Apoptosis of Malignant Human B Cells by Ligation of CD20 with Monoclonal Antibodies. Blood. 1998; 91:1644–1652. [PubMed: 9473230]

37. Ben-Bassat H, Goldblum N, Mitrani S, Goldblum T, Yoffey JM, Cohen MM, Bentwich Z, Ramot B, Klein E, Klein G. Establishment in Continuous Culture of a New Type of Lymphocyte from a "Burkitt Like" Malignant Lymphoma (Line D.G.-75). Int. J. Cancer. 1977; 19:27–33. [PubMed: 188769]

38. Johnson RN, Kopečková P, Kopeček J. Synthesis and Evaluation of Multivalent Branched HPMA Copolymer-Fab' Conjugates Targeted to the B-Cell Antigen CD20. Bioconjug. Chem. 2009; 20:129–137. [PubMed: 19154157]

39. Johnson RN, Kopečková P, Kopeček J. Biological Activity of Anti-CD20 Multivalent HPMA Copolymer-Fab' Conjugates. Biomacromolecules. 2012; 13:727–735. [PubMed: 22288884]

40. Chu T-W, Yang J, Kopeček J. Anti-CD20 Multivalent HPMA Copolymer-Fab' Conjugates for the Direct Induction of Apoptosis. Biomaterials. 2012; 33:7174–7181. [PubMed: 22795544]

41. Ghetie MA, Richardson J, Tucker T, Jones D, Uhr JW, Vitetta ES. Disseminated or Localized Growth of a Human B-Cell Tumor (Daudi) in SCID Mice. Int. J. Cancer. 1990; 45:481–485. [PubMed: 2307538]

42. Ghetie MA, Tucker K, Richardson J, Uhr JW, Vitetta ES. The Antitumor Activity of an Anti-CD22 Immunotoxin in SCID Mice with Disseminated Daudi Lymphoma Is Enhanced by Either an Anti-CD19 Antibody or an Anti-CD19 Immunotoxin. Blood. 1992; 80:2315–2320. [PubMed: 1384801]

43. Griffiths GL, Mattes MJ, Stein R, Govindan SV, Horak ID, Hansen HJ, Goldenberg DM. Cure of SCID Mice Bearing Human B-Lymphoma Xenografts by an Anti-CD74 Antibody-Anthracycline Drug Conjugate. Clin. Cancer Res. 2003; 9:6567–6571. [PubMed: 14695162]

44. Wu K, Yang J, Liu J, Kopeček J. Coiled-Coil Based Drug-Free Macromolecular Therapeutics: *In Vivo* Efficacy. J. Control. Release. 2012; 157:126–131. [PubMed: 21843563]

45. Okroj M, Österborg A, Blom AM. Effector Mechanisms of Anti-CD20 Monoclonal Antibodies in B Cell Malignancies. Cancer Treat. Rev. 2013; 39:632–639. [PubMed: 23219151]

46. Chen WC, Completo GC, Sigal DS, Crocker PR, Saven A, Paulson JC. *In Vivo* Targeting of B-Cell Lymphoma with Glycan Ligands of CD22. Blood. 2010; 115:4778–4786. [PubMed: 20181615]

47. Goodwin DA, Meares CF. Advances in Pretargeting Biotechnology. Biotechnol. Adv. 2001; 19:435–450. [PubMed: 14538068]

48. Gunn J, Park SI, Veiseh O, Press OW, Zhang M. A Pretargeted Nanoparticle System for Tumor Cell Labeling. Mol. Biosyst. 2011; 7:742–748. [PubMed: 21107453]

49. Zhou J, Soontornworajit B, Snipes MP, Wang Y. Development of a Novel Pretargeting System with Bifunctional Nucleic Acid Molecules. Biochem. Biophys. Res. Commun. 2009; 386:521–525. [PubMed: 19545539]

50. Zhang N, Khawli LA, Hu P, Epstein AL. Generation of Rituximab Polymer May Cause Hyper-Cross-Linking-Induced Apoptosis in Non-Hodgkin's Lymphomas. Clin. Cancer Res. 2005; 11:5971–5980. [PubMed: 16115941]

51. Herter S, Herting F, Mundigl O, Waldhauer I, Weinzierl T, Fauti T, Muth G, Ziegler-Landesberger D, Van Puijenbroek E, Lang S, et al. Preclinical Activity of the Type II CD20 Antibody GA101 (Obinutuzumab) Compared with Rituximab and Ofatumumab *In Vitro* and in Xenograft Models. Mol. Cancer Ther. 2013; 12:2031–2042. [PubMed: 23873847]

52. Nguyen JT, Evans DP, Galvan M, Pace KE, Leitenberg D, Bui TN, Baum LG. CD45 Modulates Galectin-1-Induced T Cell Death: Regulation by Expression of Core 2 *O*-Glycans. J. Immunol. 2001; 167:5697–5707. [PubMed: 11698442]

53. Gu Z, Yamashiro J, Kono E, Reiter RE. Anti-Prostate Stem Cell Antigen Monoclonal Antibody 1G8 Induces Cell Death *In Vitro* and Inhibits Tumor Growth *In Vivo via* a Fc-Independent Mechanism. Cancer Res. 2005; 65:9495–9500. [PubMed: 16230414]

54. Fowers KD, Callahan J, Byron P, Kopeček J. Preparation of Fab' from Murine IgG2a for Thiol Reactive Conjugation. J. Drug Target. 2001; 9:281–294. [PubMed: 11697031]

55. Pan H, Yang J, Kopečková P, Kopeček J. Backbone Degradable Multiblock *N*-(2-Hydroxypropyl)methacrylamide Copolymer Conjugates *via* Reversible Addition-Fragmentation Chain Transfer Polymerization and Thiol-Ene Coupling Reaction. Biomacromolecules. 2011; 12:247–252. [PubMed: 21158387]

56. Kopeček J, Bažilová H. Poly[*N*-(2-hydroxypropyl)methacrylamide] — I. Radical Polymerization and Copolymerization. Eur. Polym. J. 1973; 9:7–14.

57. Šubr V, Ulbrich K. Synthesis and Properties of New *N*-(2-Hydroxypropyl)methacrylamide Copolymers Containing Thiazolidine-2-thione Reactive Groups. React. Funct. Polym. 2006; 66:1525–1538.

58. Omelyanenko V, Kope ková P, Gentry C, Kope ek J. Targetable HPMA Copolymer-Adriamycin Conjugates. Recognition, Internalization, and Subcellular Fate. J. Control. Release. 1998; 53:25–37. [PubMed: 9741911]
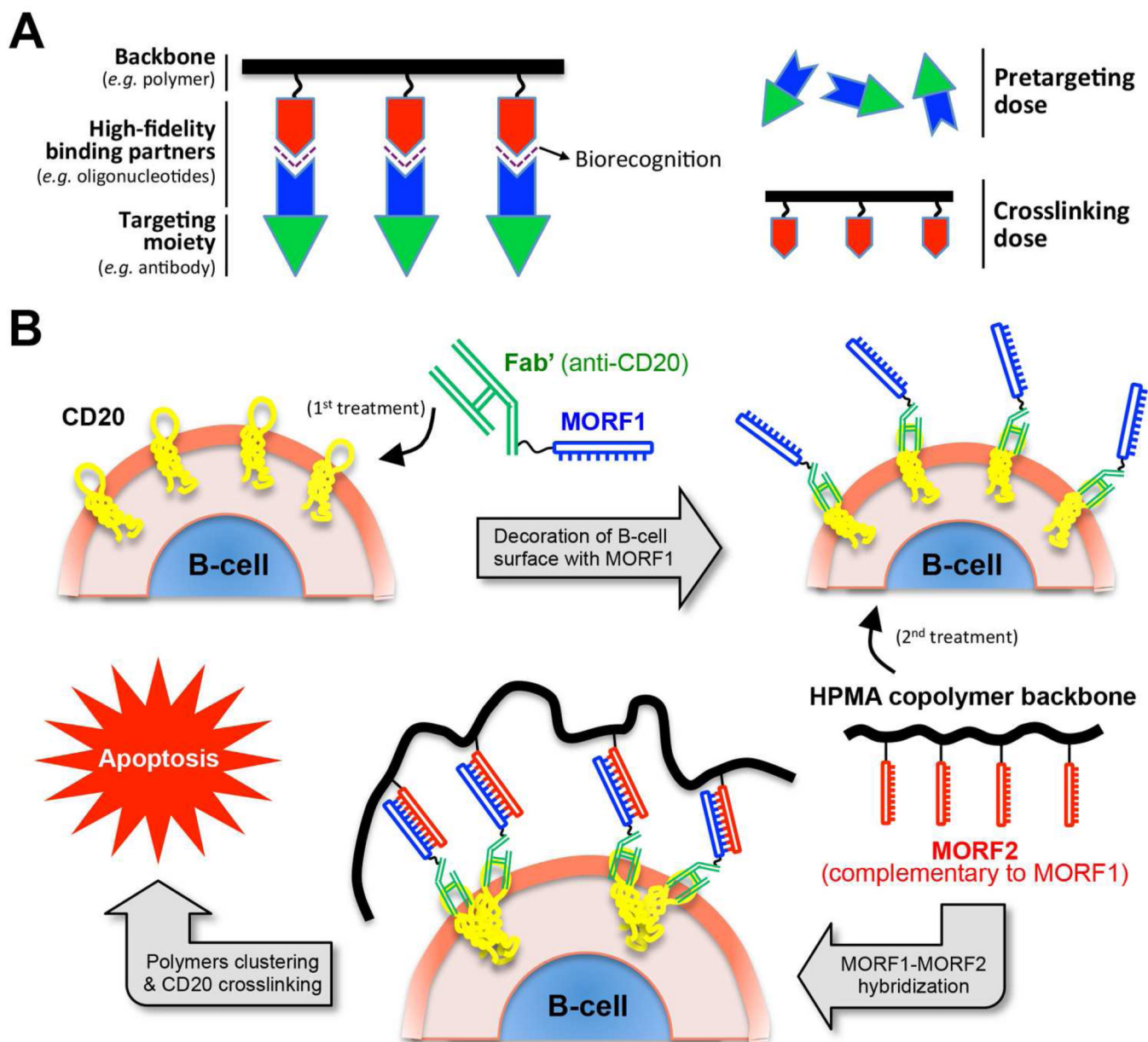
Figure 1. Self-assembling hybrid nanoconjugates for apoptosis induction
(**A**) General design concept of the therapeutic platform. Two nanoconjugates that self-assemble *via* biorecognition can be administered consecutively as pretargeting and crosslinking doses, or premixed to form a multivalent construct and used as a single dose. (**B**) Apoptosis induction of B-cells by crosslinking of the CD20 antigens that is mediated by extracellular hybridization of complementary morpholino oligonucleotides (MORF1-MORF2).
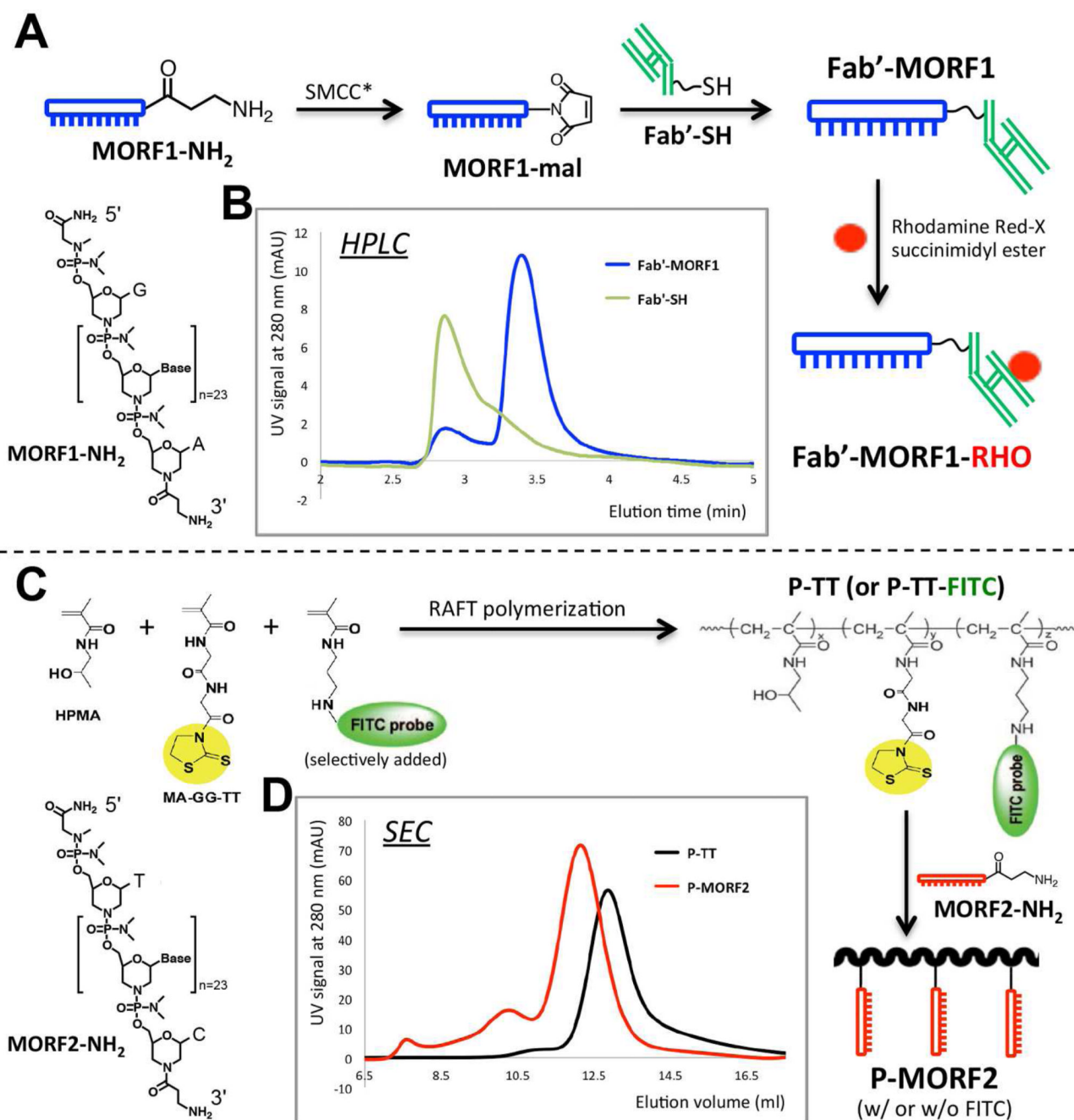
Figure 2. Synthesis and characterization of Fab'-MORF1 and P-MORF2
(**A**) Scheme of Fab'-MORF1 synthesis. *SMCC: succinimidyl-4-(*N*-maleimidomethyl)cyclohexane-1-carboxylate heterobifunctional linker. (**B**) HPLC analysis of the Fab' fragment (Fab'-SH) of 1F5 mAb and the Fab'-MORF1 conjugate; Agilent Zorbax 300SB-C18 column (4.6 × 250 mm) eluted with a gradient of buffer A (H_2O + 0.1% trifluoroacetic acid v/v) and buffer B (acetonitrile + 0.1% trifluoroacetic acid v/v). (**C**) Scheme of the synthesis of polymer precursors (P-TT) and multivalent conjugates (P-MORF2). MA-GG-TT: *N*-methacryloylglycylglycine thiazolidine-2-thione (MA-GG-TT). (**D**) SEC analysis of representative P-TT and P-MORF2 (valence=3); Superose 6 HR10/30 column (acetate buffer + 30% acetonitrile v/v).
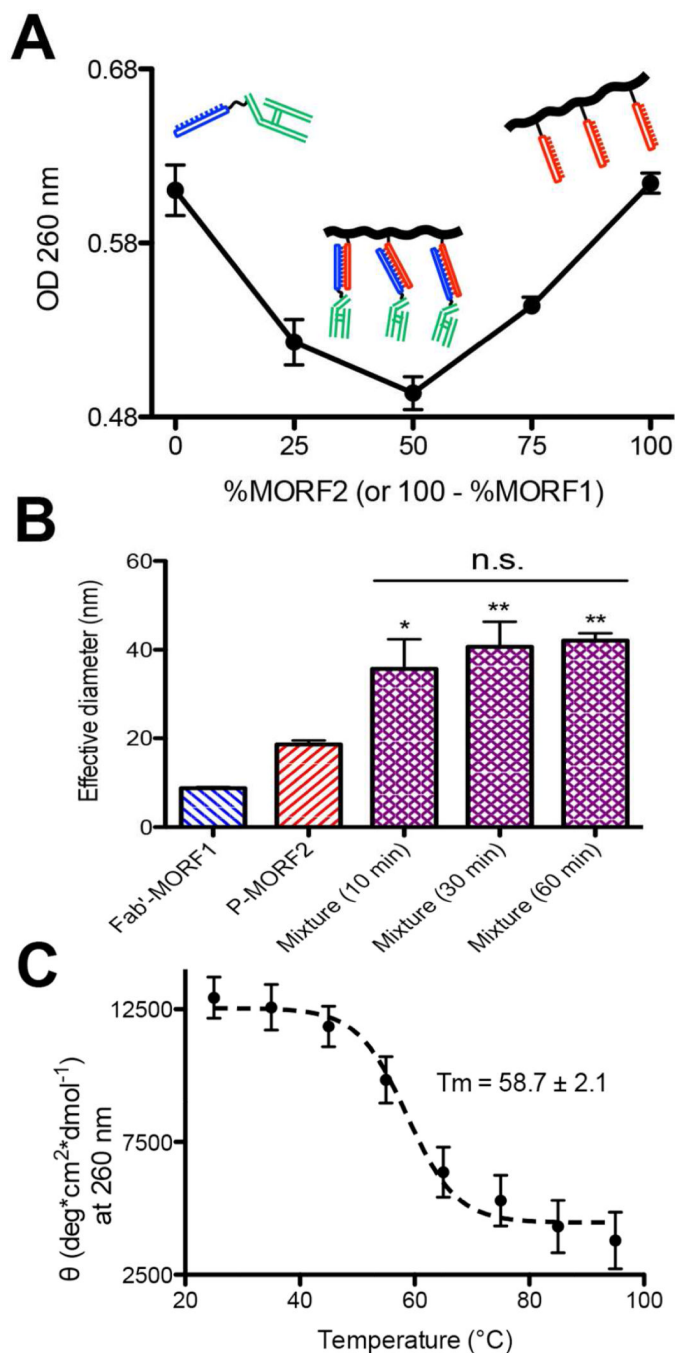
Figure 3. *In vitro* hybridization of Fab'-MORF1 and P-MORF2

(**A**) Hypochromic effect upon hybridization of Fab'-MORF1 and P-MORF2 as analyzed by UV-Vis. The optical density (OD) at 260 nm decreased when the two conjugates were mixed (in different ratios). (**B**) Effective hydrodynamic diameters of the two conjugates and their mixture (equimolar MORF1/MORF2; tested at different times after mixing) as characterized by dynamic light scattering. The valence of P-MORF2 was 3. Statistics, unless otherwise indicated, was performed by comparing the mixture with P-MORF2 (*: $p < 0.05$, **: $p < 0.005$, n.s.: no significant difference). (**C**) CD thermal melting curve of the hybridized Fab'-MORF1/P-MORF2. The molar ellipticity (θ) at 260 nm underwent a

sigmoidal decrease as temperature increased. The melting temperature (Tm) resulted from fitting the data to a logistic function using nonlinear regression (GraphPad Prism 5 software). All experiments were performed at physiological conditions (PBS, pH=7.4). Data are presented as mean ± SD (n=3).

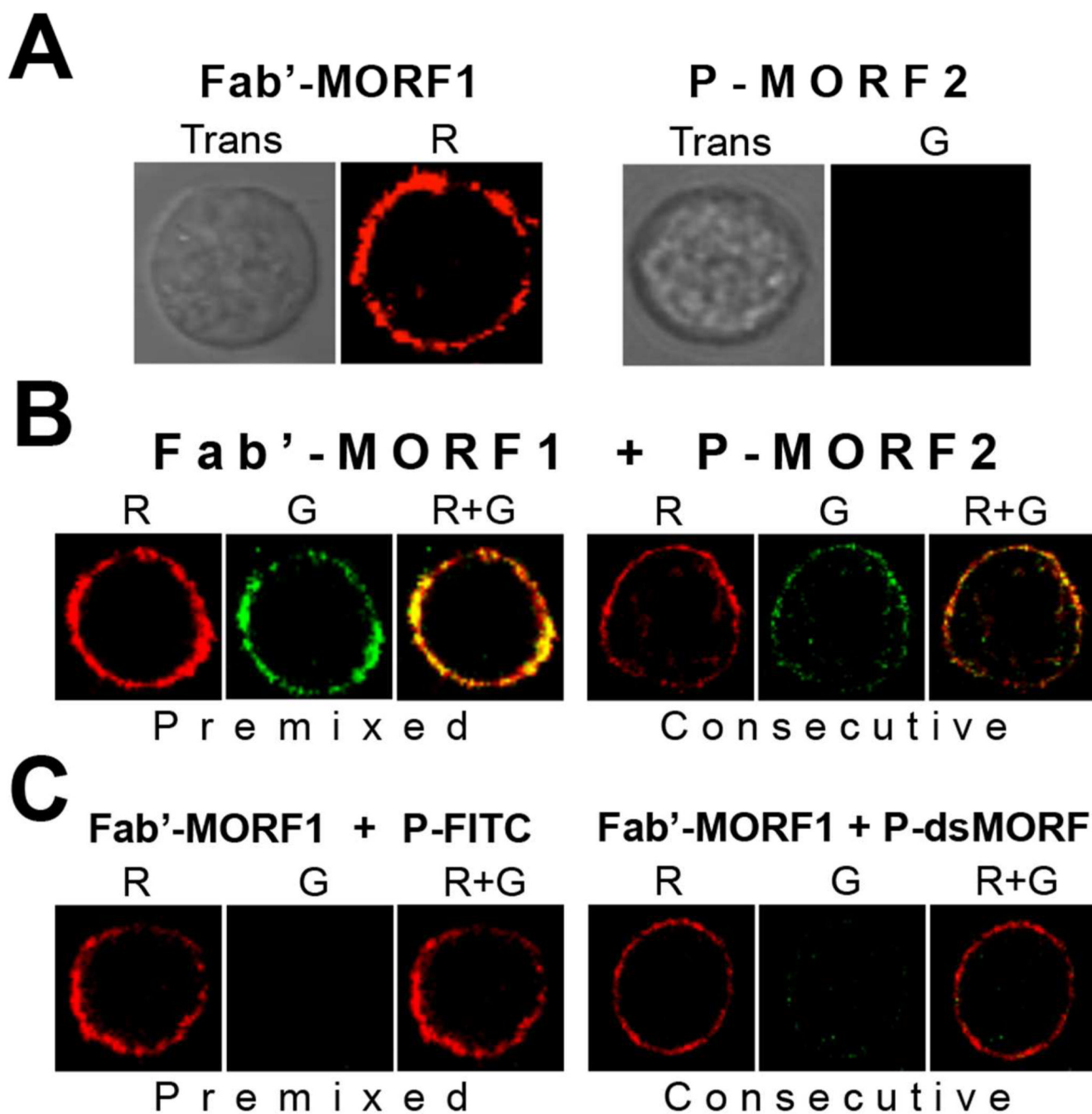**Figure 4. Biorecognition of Fab'-MORF1 and P-MORF2 at cell surface**
Confocal microscopic images of Raji B-cells (CD20^{+}) exposed to Fab'-MORF1 (labeled with rhodamine; red) and P-MORF2 (labeled with FITC; green; valence=2) are shown. Trans: images acquired under transmitted light, R: red channel, G: green channel. (**A**) Cells exposed to only Fab'-MORF1 (0.4 μM) or P-MORF2 (0.4 μM, MORF2 equivalent). (**B**) Cells exposed to the mixture of Fab'-MORF1 (0.4 μM) and P-MORF2 (0.4 μM, MORF2 equivalent) (*Premixed*), or Fab'-MORF1 first, followed 1 h later by P-MORF2 (*Consecutive*). (**C**) Control studies: (left panel) cells exposed to a premixture of Fab'-MORF1 (0.5 μM) and polymer precursors labeled with FITC (P-FITC; excess amount);

(right panel) cells exposed consecutively to Fab'-MORF1 (0.5 μM) and P-MORF2 pre-blocked by MORF1 (P-dsMORF; excess amount).
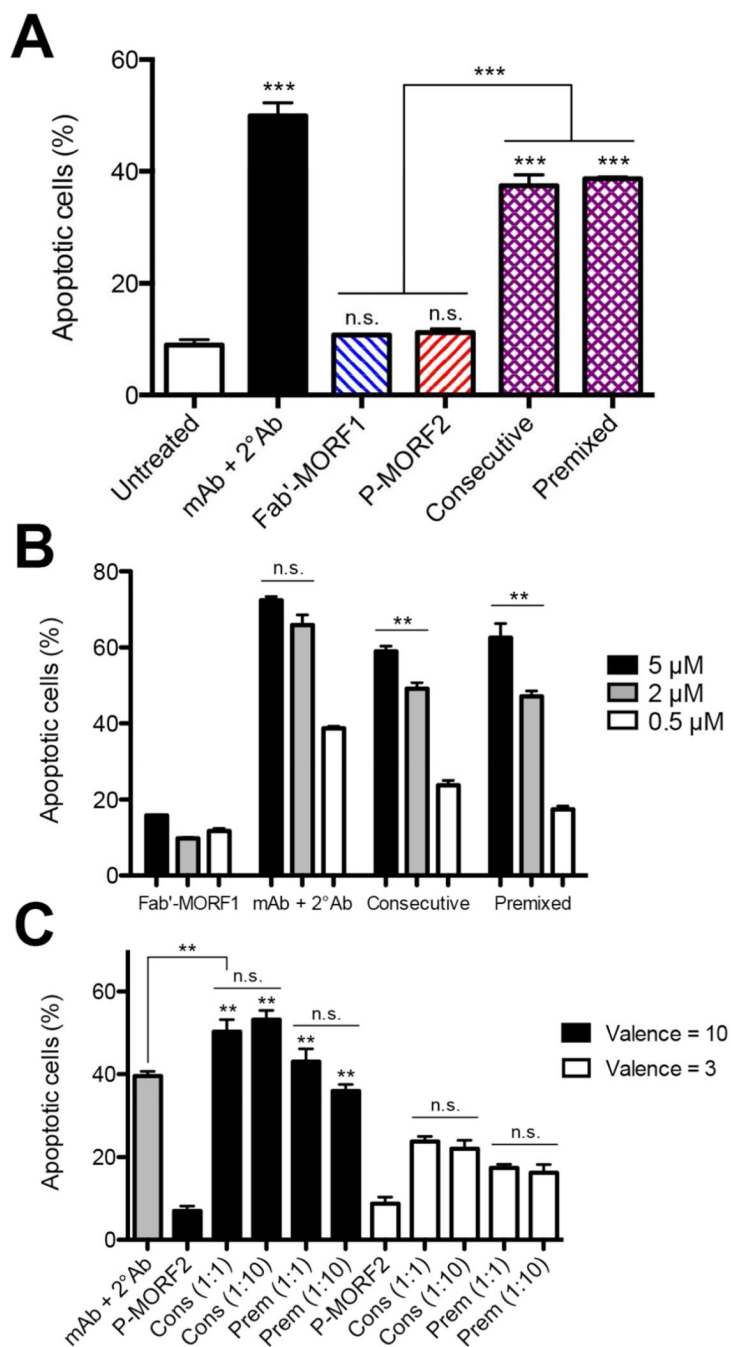
Figure 5. Apoptosis induction of Raji B-cells
Percentage of apoptotic cells were analyzed by annexin V/PI binding and quantified by flow cytometry. Incubation time was 48 h. (**A**) *Untreated*: cells in culture medium; *mAb + 2° Ab*: 1F5 mAb (1 μM) followed (1 h later) by goat anti-mouse secondary Ab (0.5 μM); *Fab'-MORF1*: single-component at 1 μM; *P-MORF2*: single-component of P-MORF2/v3 at 1 μM (MORF2-eqv.); *Consecutive*: Fab'-MORF1 (1 μM) followed (1 h later) by P-MORF2/v3 (1 μM); *Premixed*: premixture of Fab'-MORF1 (1 μM) and P-MORF2/v3 (1 μM). Statistics, unless otherwise indicated, was performed by comparing each group with untreated (***: p < 0.0001, n.s.: no significant difference). (**B**) Treatments with different concentrations of

Fab'-MORF1 (as indicated) and corresponding P-MORF2/v3 (at equimolar MORF1/MORF2). **: $p < 0.005$, n.s.: no significant difference. (**C**) Treatments with different valences of P-MORF2 (3 or 10 MORF2 per polymer chain) and different MORF1:MORF2 molar ratios (1:1 or 1:10). *Cons*: consecutive treatment of two conjugates; *Prem*: premixture of two conjugates. Concentration of Fab'-MORF1 was 0.5 μM. *P-MORF2*: single-component treatment with P-MORF2/v3 or P-MORF2/v10 at 5 μM (MORF2 equivalent); *mAb + 2° Ab*: 1F5 mAb (0.5 μM) followed by goat anti-mouse secondary Ab (0.25 μM). Statistics, unless otherwise indicated, was performed by comparing each "high-valence" group with the corresponding "low-valence" group (**: $p < 0.005$, n.s.: no significant difference). All data are presented as mean ± SD (n=3).
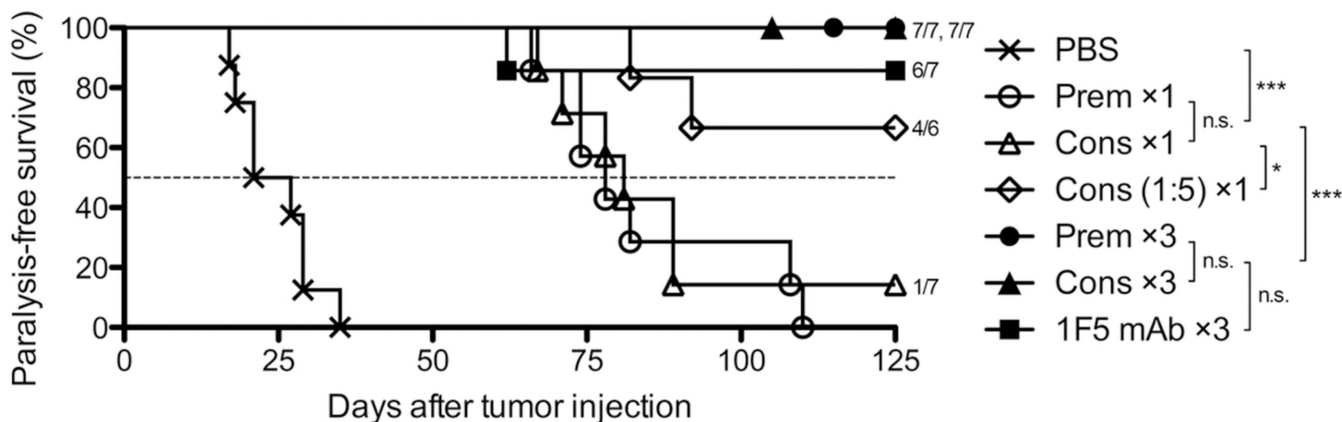
Figure 6. Therapeutic efficacy of the nanomedicine against systemic lymphoma in SCID mice
Four million Raji B-cells were injected *via* tail vein on day 0; incidence of hind-limb paralysis or survival of mice was monitored until day 125. One-dose treatment on day 1; three-dose treatment on days 1, 3, and 5. *PBS*: mice injected with PBS (n=8); *Cons ×1*: consecutive treatment of Fab'-MORF1 and P-MORF2/v10, 1-dose (n=7); *Prem ×1*: premixture of Fab'-MORF1 and P-MORF2/v10, 1-dose (n=7); *Cons (1:5) ×1*: consecutive treatment, MORF1:MORF2=1:5, 1-dose (n=6); *Cons ×3*: 3 doses of consecutive treatment (n=7); *Prem ×3*: 3 doses of premixture (n=7); *1F5 mAb ×3*: 3 doses of 1F5 mAb (n=7). The paralysis-free survival of mice is presented in a Kaplan-Meier plot. Numbers of long-term survivors in each group are indicated (if any). Statistics was performed with log-rank test (*: p < 0.05, ***: p < 0.0001, n.s.: no significant difference).
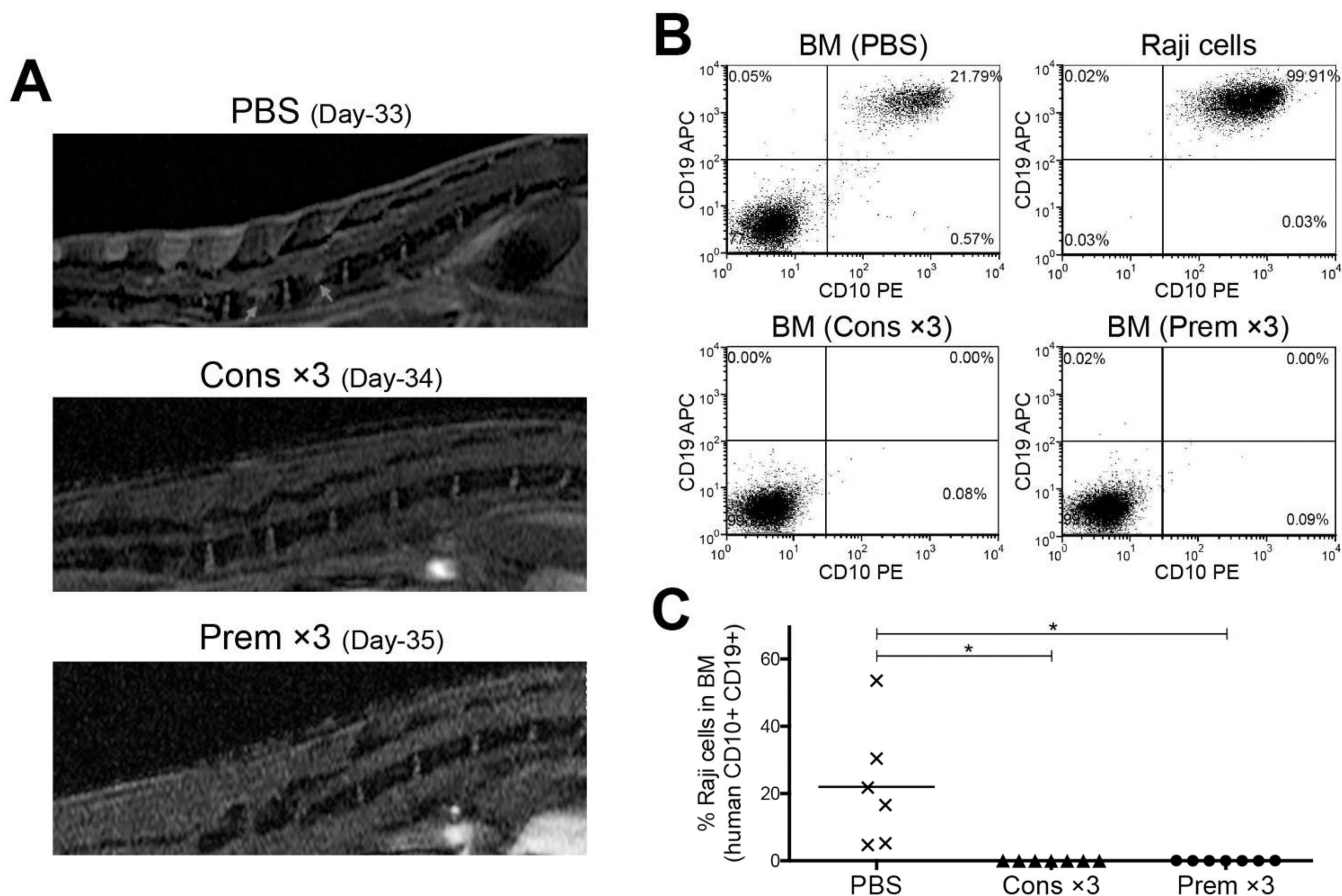
Figure 7. Eradication of Raji cells in SCID mice

Mice *i.v.* injected with 4×10^6 Raji B-cells on day 0 were exposed to different treatments – *PBS*: mice injected with PBS; *Cons ×3*: consecutive treatment of Fab'-MORF1 and P-MORF2/v10 on days 1, 3 and 5; *Prem ×3*: 3 doses of the premixture of Fab'-MORF1 and P-MORF2/v10 on days 1, 3 and 5. (**A**) Post-contrast T_1-weighted sagittal MRI focusing on the lumbar spine of mice. A heterogeneous appearance and irregularly shaped masses indicating tumor nodules (red arrows) were observed in the spinal cord of control mice (PBS, n=4), but not in the treated mice (Cons ×3 and Prem ×3, n=4). (**B**) Flow cytometry analysis of residual Raji cells in the bone marrow (BM) of the PBS-treated, paralyzed mice (PBS) and the nanomedicine-treated, surviving mice (Cons ×3, Prem ×3). Bone marrow cells isolated from the femur of mice and Raji cells from culture flasks (upper right panel) were stained with PE-labeled mouse anti-human CD10 and APC-labeled mouse anti-human CD19 antibodies. (**C**) Quantitative comparison of % Raji cells (human CD10$^+$ CD19$^+$) in the bone marrow of control mice (PBS, n=6) and the nanomedicine-treated mice (Cons ×3 and Prem ×3, n=7 per group) as analyzed by flow cytometry. Each data point represents an individual mouse; mean % is indicated. Statistics was performed by Student's *t* test of unpaired samples (*: p < 0.05).
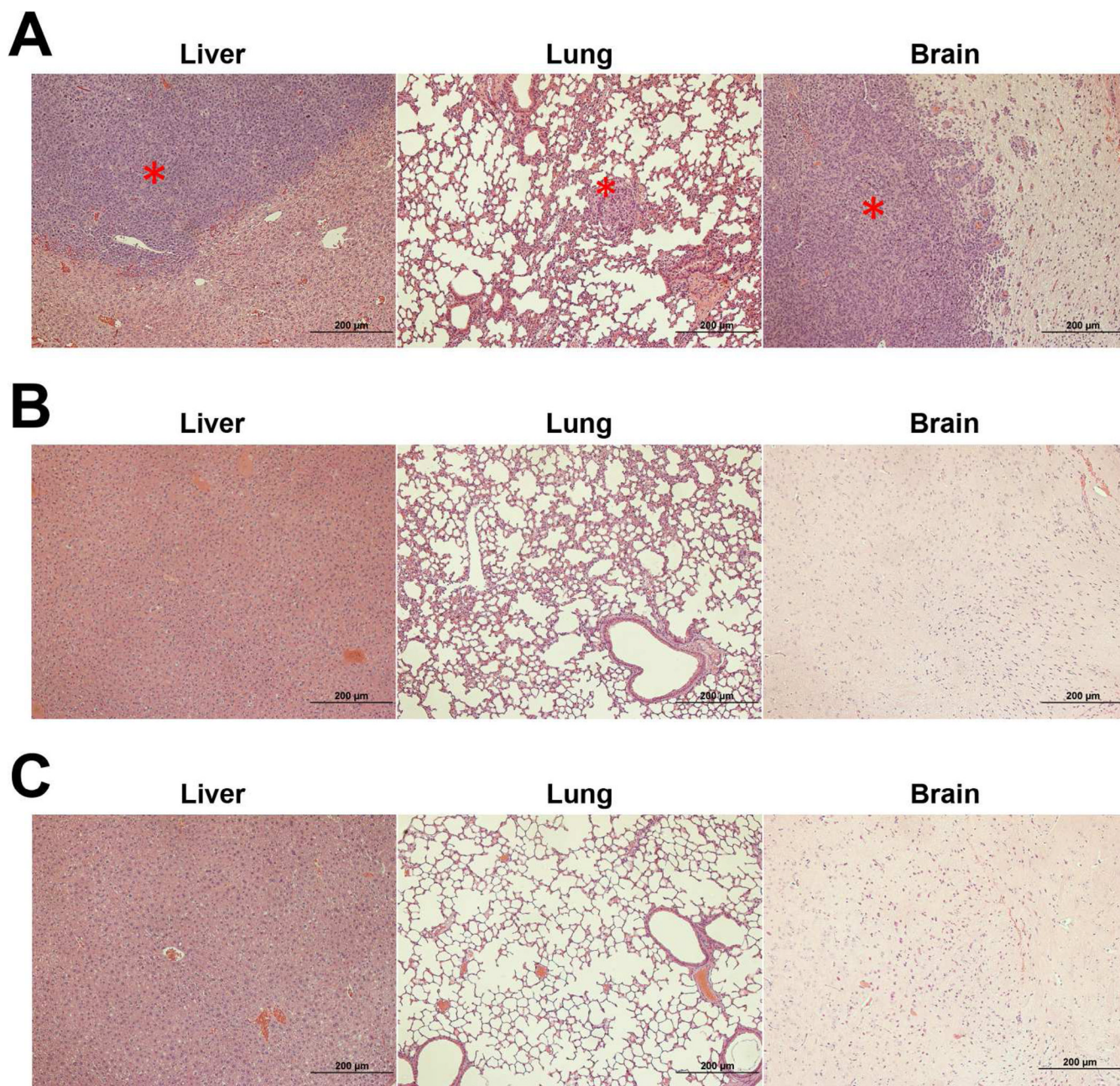
Figure 8. Histopathological examination

(**A**) Control mice that were injected with Raji cells and treated with PBS developed metastatic tumors in the liver (2 mice found with tumors/4 mice examined), lung (3/4), and brain (1/4), as demonstrated by invasion of monomorphic lymphoma cells (red asterisks) and disruption of normal tissue architecture. (**B**) Three doses of the consecutive treatment of Fab'-MORF1 and P-MORF2 (Cons ×3) resulted in no evidence of lymphoma invasion (0/3, for all organs). (**C**) Three doses of the premixed treatment (Prem ×3) prevented lymphoma dissemination (0/3, for all organs). Hematoxylin and eosin (H&E)-stained tissue specimens were examined by a blinded veterinary pathologist. No toxicity of the treatment was suggested in any of the organs evaluated.